all measurements described above were performed at 77 K for monomers and polymer aggregates of Chl *a*, fluorescence quenching has been observed in various solvents up to 273 K, well above the corresponding glass transition temperatures. A specially prepared sample which yielded almost entirely (Chl *a*·H_2O)$_2$ aggregates upon cooling to 77 K showed similar quenching behavior. Further investigation of the temperature dependence of fluorescence quenching for various aggregates is in progress.

The experimental findings and conclusions reported above have thus unraveled a primary two-photon mechanism that could conceivably play a part in (Chl a·$2H_2O$)$_n$ photoreaction with water. The secondary events of this reaction are manifested by the ESR detection of the redox reaction cycle of the light-induced (Chl a·$2H_2O$)$_n^{+\cdot}$ radical cation and by the observation of photocathodic behavior of the Pt/Chl *a*·H_2O electrode. The close similarity of the fluorescence quenching effects illustrated in Figures 5 and 6 suggests that the two-photon mechanisms discussed above for aggregated Chl *a* may also be relevant considerations in the case of monomeric hydrated Chl a complexes, although any photocatalytic effects attending this latter case have not been identified. The photoexcitation of monomeric hydrated Chl *a* delayed fluorescence, which does not result in photooxidation of the chlorophyll, is ascribable to a one-quantum process.[16] The above observations suggest the possibility that the available Chl *a* two-photon mechanism is an alternative pathway, effective in Chl *a* photochemistry only when redox requirements compatible with the water splitting reaction are satisified by a specific aggregate configuration, such as (Chl *a*·$2H_2O$)$_{n\geq 2}$. In this sense the stereospecific interactions of Chl a–H_2O interactions seem to take on an added significance in the study of the Chl *a* water splitting reaction. In view of eq 19 it is evident that, under steady-state illumination, the chlorophyll is distributed predominantly between the ground-state singlet and the CT complex and that the steady-state populations of S_1 and T_1 are negligibly low. These observations are apparently in agreement with the fact that (Chl *a*·$2H_2O$)$_n$ in homogeneous solutions is only very weakly fluorescent[16] and that in a condensed state, in which k_{ST} is expected to be significantly enhanced,[19] the chlorophyll is nonfluorescent. In this connection it is noteworthy that the fluorescent and the triplet states of the water splitting reaction center Chl *a* in vivo have hitherto not been observed.

Acknowledgment. The work reported in this paper was supported by the Basic Research Division of the Gas Research Institute.

Elementary Reconstitution of the Water Splitting Light Reaction in Photosynthesis. 3. Photooxidative Properties of Chlorophyll Dihydrate on Metal as Catalyst for Water Photolysis

Michael S. Showell and Francis K. Fong*

Contribution from the Department of Chemistry, Purdue University, West Lafayette, Indiana 47907. *Received October 14, 1981*

Abstract: In this work we investigate the photooxidative properties of chlorophyll *a* dihydrate as photocatalyst for the water splitting reaction, using Pt and other metals as nonbiological catalysts for reaction product formation. The photoelectrodeposition of (Chl *a*·$2H_2O$)$_n$ microcrystals from *n*-pentane suspensions on Pt electrodes is described. The formation of a contiguous multilayer of (Chl *a*·$2H_2O$)$_n$ on Pt is examined by means of electron microscopy. The effect of an applied voltage on the electrodeposition process is delineated in terms of the amount of Chl *a* plated and the photocathodic activity of the resulting Pt|Chl *a* electrode. A quantum efficiency of 0.88% was obtained at the red maximum, 735 nm, of the photogalvanic action spectrum. The catalytic function of the metal surface is examined by determining the activity of a Pt|Chl *a*–H_2O photocathode against a series of different counterelectrodes (anodes), viz., Pt, Cu, Fe, and Ni. The order Cu > Ni > Fe > platinized Pt > shiny Pt is established for the relative effectiveness of these metals as counterelectrodes at photocurrent densities $\gtrsim 10^{-1}$ $\mu A/cm^2$ in oxygen-depleted aqueous solutions. The observation of light-induced decay and dark restoration of the photogalvanic activity is numerically fitted to a kinetic model for gaseous product evolution and removal at the electrodes. The apparent reduction potential for a 1:3 mixture of (Chl *a*·$2H_2O$)$_2^{+\cdot}$ and (Chl a·$2H_2O$)$_6^{+\cdot}$ responsible for the observed oxygen evolution from water splitting is determined by potentiostatic and electron spin resonance measurements to be 1.05 V. This observation is attributable to the reduction potential of (Chl *a*·$2H_2O$)$_n^{+\cdot}$.

Photosynthesis in green plants involves two different chlorophyll–protein complexes known as the "P700" and the "P680" reaction centers. The latter is commonly recognized to be directly responsible for the evolution of molecular oxygen from the water splitting reaction in vivo. In recent years there has been an increasing number of investigations in light conversion and photon energy storage using the chlorophyll as photocatalyst in the absence of biological enzymes.[1-14] Observations on the in vitro photosynthetic activity of Chl *a* show that the dimers of chlorophyll *a* monohydrate and dihydrate, (Chl a·H_2O)$_2$ and (Chl *a*·$2H_2O$)$_2$,

(1) T. Miyasaka and K. Honda, in "Photoeffects at Semiconductor-Electrolyte Interface", A. J. Nozik, Ed., American Chemical Society, Washington, DC, 1981, Adv. Chem. Ser. No. 146, p 231.
(2) F. K. Fong, in "Light Reaction Path of Photosynthesis", F. K. Fong, Ed., Springer-Verlag, Heidelberg, West Germany, Chapter 8, in press.
(3) C. W. Tang, F. Douglas, and A. C. Albrecht, *J. Phys. Chem.*, **79**, 2723 (1975).
(4) C. W. Tang and A. C. Albrecht, *J. Chem. Phys.*, **63**, 953 (1975).
(5) J. G. Villar, *J. Bioenerg. Biomembr.*, **8**, 199 (1976).
(6) J. M. Mountz and H. T. Tien, *Photochem. Photobiol.*, **288**, 395 (1978).
(7) H. Ochiai, H. Shibata, A. Fujishima, and K. Honda, *Agric. Biol. Chem.*, **43**, 881 (1979).
(8) T. Miyasaka, T. Watanabe, A. Fujishima, and K. Honda, *Nature (London)*, **277**, 638 (1979).
(9) F. K. Fong and N. Winograd, *J. Am. Chem. Soc.*, **98**, 2287 (1976).
(10) F. Takahashi and R. Kikinchi, *Biochim. Biophys. Acta*, **430**, 490 (1976).
(11) Y. Toyoshima, M. Morino, H. Motoki, and M. Sukigara, *Nature (London)*, **265**, 187 (1977).
(12) T. Miyaska, T. Watanabe, A. Fujishima, and K. Honda, *J. Am. Chem. Soc.*, **100**, 6657 (1978).

0002-7863/82/1504-2773$01.25/0

respectively, display photochemical and photophysical properties analogous to those attributed to the P700 and the water splitting reactions in plant photosynthesis.[15] Of particular interest is the ability of (Chl a·$2H_2O$)$_{n\geq 2}$, when plated in multilayers on Pt surfaces, to photocatalyze water cleavage[16]

$$2H_2O \xrightarrow[(\text{Chl } a\cdot 2H_2O)_n]{h\nu} 2H_2 + O_2 \quad (1)$$

and CO_2 photoreduction[17]

$$2H_2O + CO_2 \xrightarrow[(\text{Chl } a\cdot 2H_2O)_n]{h\nu} CH_2O + H_2O + O_2 \quad (2)$$

$$2CO_2 + 2H_2O \xrightarrow[(\text{Chl } a\cdot 2H_2O)_n]{h\nu} 2H_2CO_2 + O_2 \quad (3)$$

In papers 1 and 2 of this series we examined the physical and photochemical properties of hydrated Chl a light reaction with water in the absence of biological enzymes and/or nonbiological catalysts. In this paper we attempt to elucidate the experimental behavior of Chl a as photocatalyst for the above oxygen evolving reactions using metal surfaces as catalytic agents for liberation of the gaseous products.

Reactions 1–3 are obtained on illumination of platinized (Chl a·$2H_2O$)$_n$ electrodeposited on Pt.[16,17] The photocatalytic assembly in this case consists of (Chl a·$2H_2O$)$_n$ multilayers sandwiched in Pt. In a different experimental configuration, in demonstrating the photogeneration of electricity using visible light, the (Chl a·$2H_2O$)$_n$ multilayer deposited on the platinum is not coated by an outer layer of Pt black. In photochemical conversions the counterelectrode is placed in a second half-cell separated from the Pt/Chl a electrode by a salt bridge according to the arrangement[14]

$$\text{counterelectrode}|H_2O,\ 0.1\ M\ KCl||0.1\ M\ KCl,\ H_2O|(\text{Chl } a\cdot 2H_2O)_n|Pt \quad (4)$$

Reaction 1 is thus described in terms of its corresponding half-cell reactions, and water splitting occurs concomitantly with the production of electricity through an external circuit in photogalvanic action:[14]

$$\text{Pt/Chl } a \text{ photocathode} \quad 2H_2O + 2e^- \rightarrow H_2 + 2OH^- \quad (5)$$

$$\text{Chl } a \text{ free anode} \quad 2H_2O \rightarrow 4H^+ + O_2 + 4e^- \quad (6)$$

Reactions 1–3 were characterized by means of product analysis using mass spectrometry.[16,17] The engagement of the half-cell reactions, 5 and 6, in photogalvanic action provides a convenient tool for monitoring the photoelectrochemical behavior of the chlorophyll in reactions 1–3.

Compared to monomeric Chl a, which readily undergoes photodegradation, (Chl a·$2H_2O$)$_n$ is apparently indestructible[17] under the conditions reported for the observation of reactions 1–3.[16,17] The stability of (Chl a·$2H_2O$)$_n$, of course, is essential to its function as photocatalyst. However, little is known of the molecular parameters that underlie the observed effects. The mechanisms underlying the evolution of H_2 and O_2 in reaction 1 apparently differ from those in conventional electrolysis. The appearance of the pronounced D^+ line in the mass spectrometric determination of reactions 1–3 using D_2O, observed in Chl a-catalyzed photolysis but not in conventional electrolysis,[16,17] suggests the assimilation of hydrogen radicals produced in reaction 1 by CO_2 in the photosynthesis of polyatomic molecules.[17] Observations of the scavenging of H· radicals by gaseous CO_2 in the presence of Hg have been made earlier by Ausloos and Gordon.[18] It seems reasonable to suppose that, in place of enzymes in plant photosynthesis, Pt provides a catalytic surface for the photogeneration and transfer of H atoms and OH radicals from water splitting, setting the stage for subsequent pathways of recombinations to give H_2 and O_2 and/or reaction with other chemical species present in the photoreaction apparatus. These competitive pathways form the basis for a comparative study of photosynthesis in vitro and in vivo.[2]

In the present investigation we study the photogalvanic action of the metal–(Chl a·$2H_2O$)$_n$ electrode in order to delineate the photocatalytic properties of the chlorophyll. The Pt|Chl a–H_2O electrode is prepared by electroplating (Chl a·$2H_2O$)$_n$ onto a Pt foil using a procedure similar to that described by Tang and Albrecht.[19] The (Chl a·$2H_2O$)$_n$ electroplating procedure is examined with the chlorophyll plating solution illuminated by visible light or kept in the dark. The size and physical state of the (Chl a·$2H_2O$)$_n$ crystals electroplated on Pt are determined by electron microscopy and quantitative analysis of the plating current in terms of the number of Chl a molecules electrodeposited on the platinum. The role of the metal electrode in reaction 1, discussed in connection with the overvoltage of gaseous O_2 evolution, is probed by comparing the performance characteristics of four different metals, Pt, Cu, Fe, and Ni, interchangeably employed as the counterelectrode (anode). The photogalvanic current derived from reaction 1 is examined as a function of the density of Chl a molecules and the potential field employed in the electrodeposition procedure. The effect of light on the long-term stability of the photogalvanic cell is investigated by using a kinetic model for O_2 and H_2 production. The Chl a photo-EMF is evaluated by means of potentiostatic and electron spin resonance measurements, providing a quantitative determination of the chlorophyll redox potential in terms of the molecular parameters of the hydrated Chl a aggregate radical cations. It is shown that the choice of reference half-cell in delineating the photoelectrochemical properties of the Chl a water splitting reaction is critical on account of the multiplicity of Chl a redox couples and the reaction pathway dependence on the chlorophyll's aggregation state.

Experimental Procedure

Chlorophyll a dihydrate microcrystals were prepared and purified[20] from acetone extracts of spinach leaves according to the method described by Brace et al.[21] Absorption spectra were measured on a Cary 14 spectrophotometer. Pt electrodes were prepared by spot welding a Pt wire to a 0.8 × 1.2-cm^2 Pt foil. The shiny Pt electrodes were cleaned in boiling aqua regia for 10 min. The Cu, Ni, and Fe counterelectrodes, 1.0 × 1.0 cm^2 in dimensions and spot welded to Pt wires, were cleaned by immersion in boiling concentrated HCl solutions for 2 min followed by rinsing in doubly distilled water. Pt/Chl a electrodes were prepared by electrodeposition of (Chl a·$2H_2O$)$_n$ onto a 0.8 × 1.2-cm^2 rectangular Pt foil under illumination from a visible light source. The Pt foil, whose four corners were rounded off to maximize uniformity of the plating field, was negatively charged under the influence of a dc electric field. The plating chamber was an Al block with trough dimensions 2.3- × 1.7- × 1.9 cm. The Chl a/n-pentane plating solution contained 5 × 10^{-3} M Chl a. For the field dependence study of the plating procedure, a 2-mW Coherent Radiation He–Ne laser was employed for studying the effects of light intensity and wavelength on the plating procedure. A laser beam expander was used to provide a broad, uniform photon field on the plating solution. In this case the plating chamber consists of two Cu walls on opposite sides, a mirrored back-wall to reflect the incident light, and a glass front and bottom. The dimensions for this cell were 2.7- × 2.4- × 2.4 cm. All Pt/Chl a electrodes were equilibrated at 60 °C in doubly distilled water for 2 h prior to use in the photogalvanic experiment. The photogalvanic cell was deoxygenated by flushing with Ar gas in the dark. All experiments were carried out at pH 6.2.

The apparatus used to measure the Chl a plating current is shown in Figure 1. The voltage and light sources, built in this laboratory, were

(13) F. K. Fong, *Proc. Natl. Acad. Sci. U.S.A.*, **71**, 3692 (1974); F. K. Fong and V. J. Koester, *Biochim. Biophys. Acta*, **423**, 52 (1976).
(14) F. K. Fong, J. S. Polles, L. Galloway, and D. R. Fruge, *J. Am. Chem. Soc.*, **99**, 5802 (1977).
(15) F. K. Fong, A. J. Hoff, and F. A. Brinkman, *J. Am. Chem. Soc.*, **100**, 619 (1978).
(16) F. K. Fong and L. Galloway, *J. Am. Chem. Soc.*, **100**, 3594 (1978); L. Galloway, D. R. Fruge, G. M. Haley, A. B. Coddington, and F. K. Fong, *J. Am. Chem. Soc.*, **101**, 229 (1979).
(17) D. R. Fruge, G. D. Fong, and F. K. Fong, *J. Am. Chem. Soc.*, **101**, 3694 (1979).
(18) P. Ausloos and R. Gordon, *J. Chem. Phys.*, **65**, 1033 (1961).
(19) C. W. Tang and A. C. Albrecht, *Mol. Cryst. Liq. Cryst.*, **25**, 53 (1974).
(20) H. H. Strain, M. R. Thomas, and J. J. Katz, *Biochim. Biophys. Acta*, **75**, 306 (1963).
(21) J. Brace, F. K. Fong, D. H. Darweik, V. J. Koester, A. Shepard, and N. Winograd, *J. Am. Chem. Soc.*, **100**, 5203 (1978).

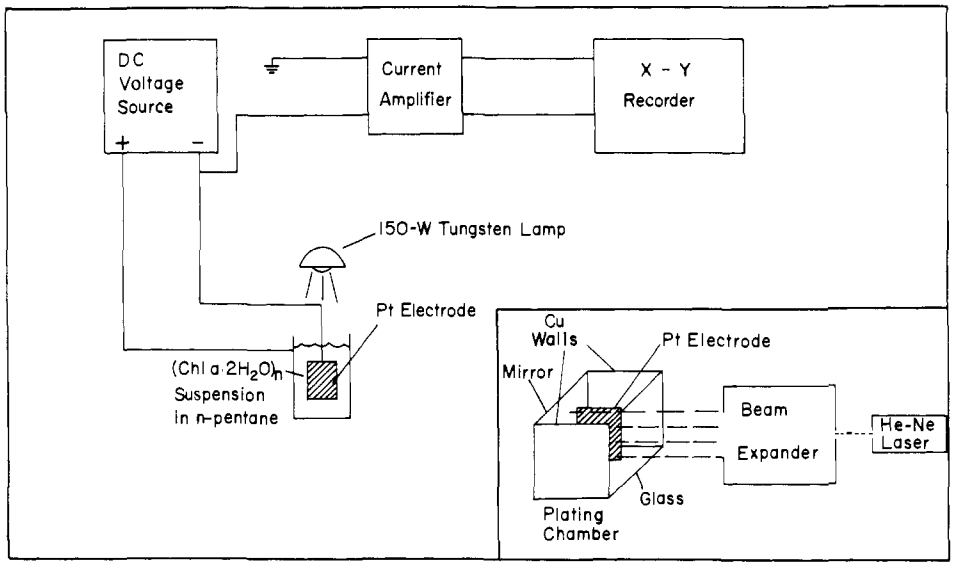

Figure 1. Experimental apparatus for measuring plating currents in the electrodeposition procedure. The dc voltage source and 150-W tungsten lamp are switched on simultaneously for the light-on experiment.

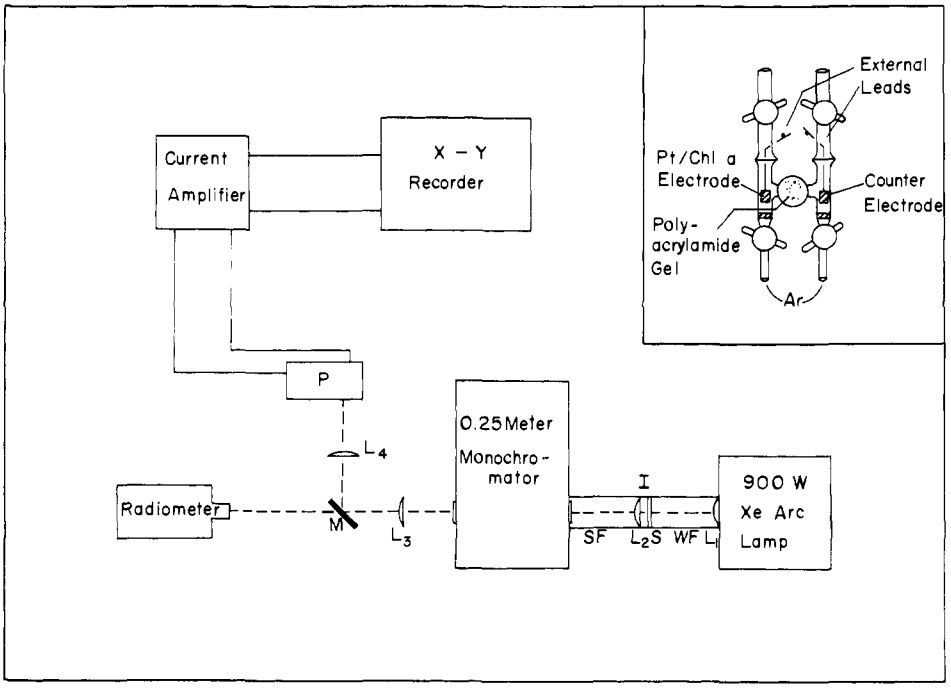

Figure 2. Schematic representation of the photogalvanic action spectrometer: L_1–L_4, lenses; WF, 8.0-cm water filter; S, shutter; I, iris; SF, spatial filter; P, photogalvanic cell; M, fixed mirror matched to chopper blade; R, radiometer. Details of the photogalvanic assembly are shown in the inset.

switched on simultaneously and the resulting current flow from ground to the Pt electrode was recorded. The corresponding amounts of Chl *a* plated were measured, through calibration against standard solutions, by Cary 14 spectrophotometric analyses of ether solutions of Chl *a* washed off the Pt/Chl *a* electrodes.

The setup of the photogalvanic experiment is schematically shown in Figure 2. The photogalvanic cell consisted of two half-cells separated by a polyacrylamide gel, one containing the Pt/(Chl *a*·$2H_2O$)$_n$ electrode and the other a Chl *a*-free counter electrode. The upper compartments of the half-cells were equipped with ground glass joints for connection to the inlet system of a Consolidated Electrodynamics Corporation 21-110-B mass spectrometer for product analysis. A 0.1 M KCl solution was employed as the electrolyte. The cell was deoxygenated by purging with Ar gas for 30 min in total darkness. A 900-W xenon arc lamp was used as the light source. A Keithley model 427 current amplifier and a Hewlett-Packard model 7030AM *x*–*y* recorder were used to measure and record the photocurrents. Procedures for mass spectrometric analyses of the gaseous products obtained in the two half-cells of the photogalvanic experiment using D- and ^{18}O-enriched water were the same as those described[16,17] elsewhere for the product analysis of reactions 1–3 using a single cell containing the platinized Pt/(Chl *a*·$2H_2O$)$_n$ electrode. The photogalvanic action spectra were obtained by using a Laser Precision Corp. Model RK 3440 pyroelectric radiometer for calibrating the incident photon fluxes. At 735 nm, the red maximum of the photogalvanic spectrum, an average power of 0.46 mW was obtained after passing the incident source through a model 82-410 Jarrell-Ash 0.25-m grating monochromator.

Oscillographs of the photogalvanic current were obtained by replacing the *x*–*y* recorder of Figure 2 with a Tektronix Type 549 storage oscilloscope and C-12 camera attachment. The radiometer of Figure 2 was replaced with a photodiode, and its output was used to trigger the oscilloscope operating in a storage mode. The excitation source was pulsed by a Bowers model 322 Chopper at 200 Hz. The light pulse and 735-nm photogalvanic current thus displayed on the oscilloscope screen were then photographed.

Electron micrographs of the Pt/Chl *a* electrode surfaces were obtained by an imaging technique. The samples were plated with Pt at an angle of 25° using an NRC 720 vacuum coater. A carbon matrix was then plated over the entire electrode surface by sputtering graphite at an angle of 90°. The chlorophyll was removed from the electrode surface with

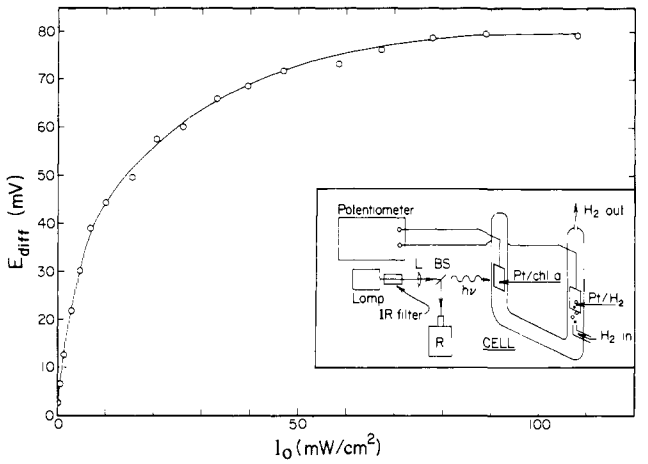

Figure 3. Flux dependence of Chl $a^{+\cdot}$ reduction potential using the hydrogen elecrode as anode. Inset: Experimental setup for measuring Chl $a^{+\cdot}$ reduction potential—IR filter, 6-in. water filter; L, lens; BS, beam splitter; R, radiometer.

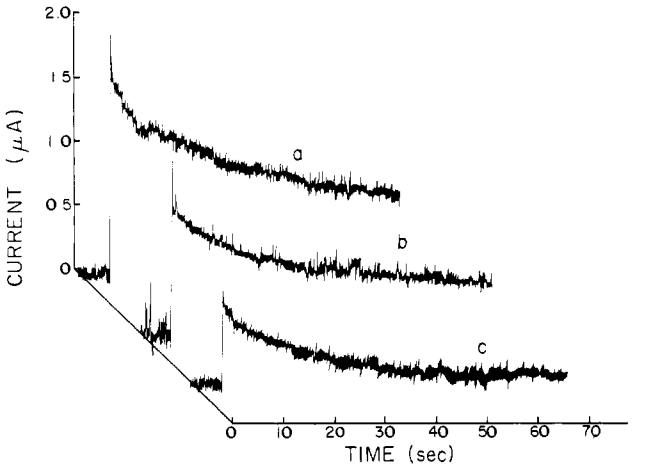

Figure 4. Plots of plating current vs. time for the deposition of (Chl $a{\cdot}2H_2O)_n^{+\cdot}$ on Pt from a 5×10^{-3} M *n*-pentane suspension of microcrystalline (Chl $a{\cdot}2H_2O)_n$: (a) Under illumination by a 150-W tungsten lamp; (b) in the dark. The corresponding blank signal, obtained from *n*-pentane not containing Chl *a*, is shown in (c).

anhydrous ethyl ether, leaving a matrix which held a replica of the Chl *a* surface. The matrix was removed from the shiny Pt electrode by immersion in doubly distilled water. Fragments of the matrix floated to the water surface and were retrieved on 200 mesh Cu sample grids. Electron micrographs were obtained from a Philips EM 300 electron microscope.

Electron spin resonance (ESR) spectra were recorded on a Varian E-line spectrometer. The Chl *a* samples were prepared in standard (3.2-mm i.d.) quartz tubes. Aliquouts of stock Chl *a* solutions in *n*-pentane ([Chl *a*] = 2.15×10^{-4} M) were transferred to the sample tubes and dried under vacuum for 1 h. Water-saturated *n*-pentane was vacuum distilled into the samples to yield Chl *a* solutions in the concentration range 1×10^{-3} to 3.2×10^{-4} M. The tubes were then flamed off under vacuum. A standard of 1.3×10^{-2} M DPPH (α,α-diphenyl-1-picrylhydrazyl) in KCl was used to measure the *g* values and concentrations of paramagnetic species in each Chl *a* sample.

Both light and dark ESR spectra were recorded in the presence and absence of H_2. The data were then digitized and fed into a CDC-6000 computer to obtain peak areas and light-minus-dark spectra. The incident flux under light conditions was 104 mW/cm^2. Heating effects were avoided by thermostating of the EPR cavity using the associated variable temperature equipment. The spectra were recorded at a mean temperature of 20.4 ± 0.5 °C.

The reduction potential of photooxidized Chl *a* was measured in a 0.5 M KCl solution at pH 6.2 under 1 atm of O_2. The cell, $Pt|H_2-H_2O$, 0.5 M KCl–(Chl $a{\cdot}2H_2O)_n|Pt$, is activated with the Pt/Chl *a* electrode illuminated by a 1000-W tungsten–halogen lamp (see inset, Figure 3). The Pt electrodes were electroplated with Pt black by passage of a 30-mA current through a 7×10^{-2} M chloroplatinic acid solution for 10 min and then rinsed with doubly distilled water. The chlorophyll was electrodeposited under illumination onto one of the Pt electrodes from a 2.15×10^{-4} M solution of Chl *a* in water-saturated *n*-pentane. The Chl *a* density on the electrode was 2.8×10^{17} molecules/cm^2. The hydrogen used for the counterelectrode was research grade purity from Airco.

The EMF's developed from this arrangement were measured, as a function of the incident light flux, on a model 8687 Leeds and Northrup potentiometer. The incident photon flux at the Pt/Chl *a* electrode was measured as described above. The cell temperature was maintained at 25.3 °C with a Haake temperature controlled water bath. Infrared radiation was filtered out by using a 6-in. water filter.

Experimental Results

In Figure 4 plots of plating current vs. time, obtained with a constant 780-V/cm field applied across the Al walls of the plating chamber and the Pt foil (inset, Figure 1), are shown for Pt/Chl *a* electrodes prepared under light and dark conditions. No measurable current flow between the Pt foil and the Al walls was obtained across the *n*-pentane/(Chl $a{\cdot}2H_2O)_n$ suspension. The observed cathodic current, shown in Figure 4, resulted instead from electron flow from ground to the Pt electrode. Figure 4c shows the current obtained with water-saturated *n*-pentane in the absence of Chl *a*. Figure 4a reproduces the measured current, obtained on illumination with an unfocused 150-W tungsten lamp, of a water-saturated *n*-pentane suspension of (Chl $a{\cdot}2H_2O)_n$. The area

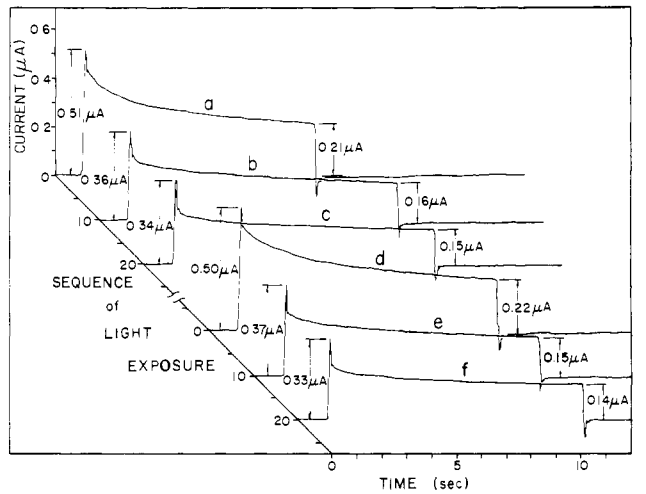

Figure 5. Sequence of experiments demonstrating the dark restoration of light-induced decay of photogalvanic activity.

under the curve over a 65-s period is 54.9 μA·s. Figure 4b shows the corresponding current measured on electroplating under identical conditons except that the chlorophyll is kept in the dark. The area under the curve over 65 s is 29.7 μA·s. The above values were corrected for the charging effects shown in Figure 4c. The amounts of Chl *a* deposited on the electrodes corresponding to the plating currents in Figure 4, a and b, were found to be 1.33×10^{17} and 7.1×10^{16} molecules/cm^2, respectively.

The photogalvanic activity of a freshly assembled cell deoxygenated in total darkness is shown in Figure 5a. The data correspond to the photocurrent obtained on exposure of the Pt/Chl *a* electrode to 735-nm light for a 10-s period. An initial current of 0.51 μA was observed followed by decay to a steady-state value of 0.21 μA. After the 10-s exposure the cell was left in the dark for 50 s prior to another 10-s exposure to the 735-nm light. The repetitive process is recorded in Figure 5, b and c, corresponding to the 10th and 20th exposures, to illustrate the effect of light on the activity of the photogalvanic cell. It was observed (Figure 5a–c) that both the initial and steady-state photocurrents decay to lower values on repeated exposures of the Pt/Chl *a* electrode to light. On flushing the cell from Figure 5c with Ar gas in the dark for 30 min, the photogalvanic activity was restored to its original value. Light-exposure experiments on the restored cell, conducted in a manner identical with that described above for Figure 5a–c, are illustrated in Figure 5d–f. One observes that the sequence of events thus obtained appear to be indistinguishable from the original series of experiments in Figure 5a–c. Mass

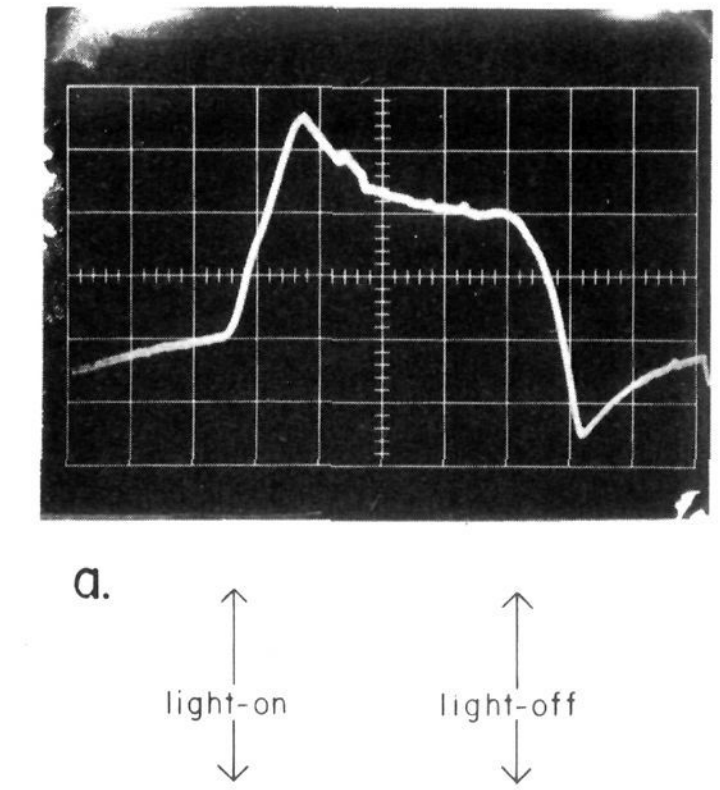

Figure 6. Oscillographic traces of the photocathodic activity in the millisecond domain: (a) photogalvanic current at 0.2-V/cm vertical gain; (b) 735-nm excitation pulse used to obtain the photocurrent in a, vertical gain = 0.5 V/cm. Sweep = 1 ms/cm.

spectrometric product analysis of the half-cell reactions in D- and ^{18}O-enriched water after 30 min of continuous illumination by visible light from the xenon-arc lamp confirmed the presence of molecular hydrogen and oxygen in both of the two half-cells, indicative of the diffusion of gaseous products from both electrodes. From calibration against conventional electrolysis we obtained a water photolysis rate of $\sim 10^{-7}$ mol/h.

In Figure 6a the oscillograph of the photogalvanic current resulting from a 735-nm excitation pulse is shown. The response time of the photodiode is ~0.01 ms compared to 0.1-ms rise time for the current amplifier. The photogalvanic signal is characterized by a ~1-ms rise to the maximum value followed by a ~2.5-ms decay to a steady-state current of ~70 nA. The temporal profile of the excitation pulse is displayed in Figure 6b.

The spectral distributions of photocathodic currents of a typical Pt/Chl *a* electrode, observed by using four different metals, Cu, Ni, Fe and Pt, as counterelectrodes, are given in Figure 7. Between measurements, on replacement of one counterelectrode with another, the cell was degassed with Ar gas for 30 min in the dark according to the restoration procedure given in Figure 5. The data points, measured beginning at the long-wavelength end and moving progressively toward the blue of a given action spectrum, correspond to a 3-s exposure of the Pt/Chl *a* electrode to establish the initial maximum photocurrents (Figure 5). The comparison in Figure 7 of the photocurrents in the Soret region, corresponding

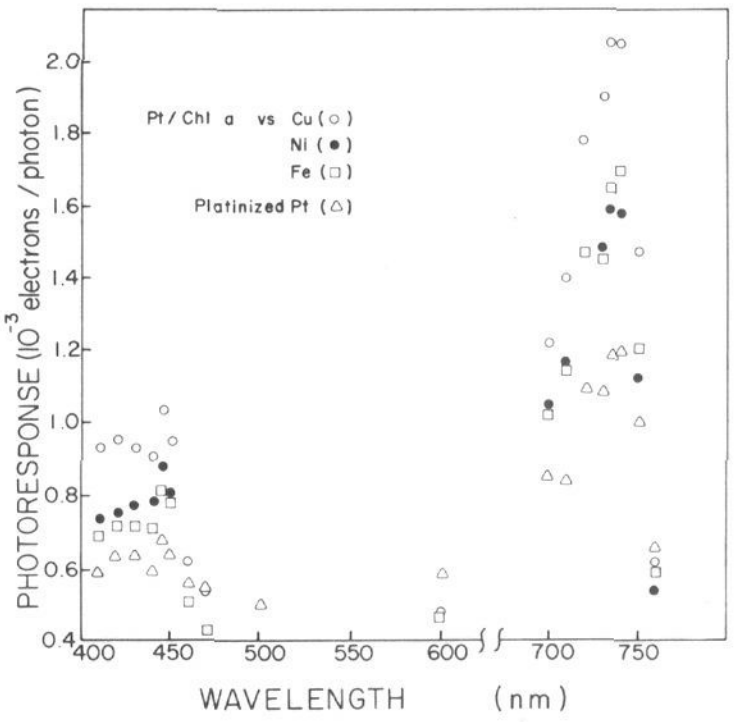

Figure 7. Dependence of the photocathodic activity of a single Pt/Chl *a* electrode on the metal employed as the dark counterelectrode (anode).

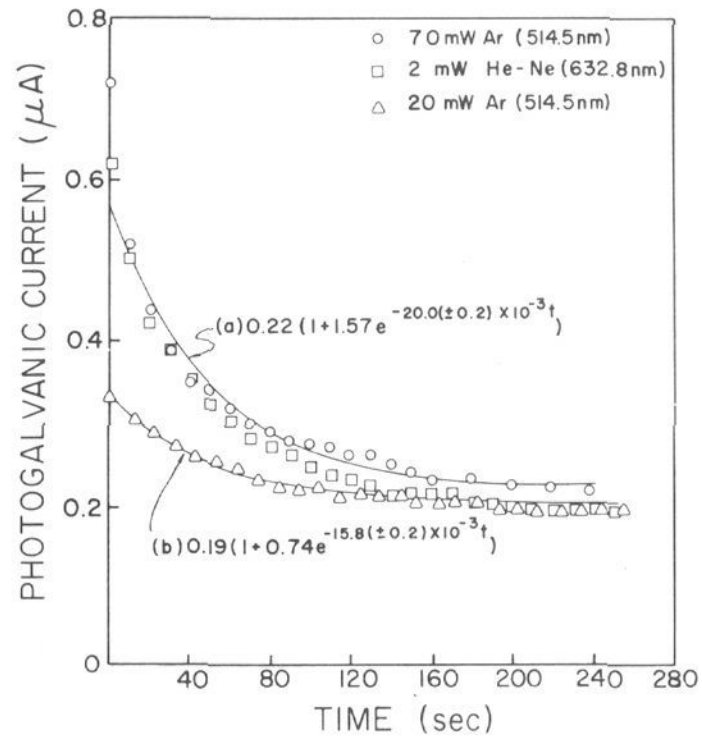

Figure 8. Light-induced decay of the ac component photocathodic signal from Pt/Chl *a* electrodes, prepared at 1300 V/cm under different illumination conditions, against a Cu counterelectrode: (○) electrode plated under illumination by a 70-mW Ar ion line at 514.5 nm; (△) electrode plated with light from a 20-mW Ar ion line at 514.5 nm; (□) electrode plated uner a 2-mW He–Ne laser beam at 632.8 nm.

to the stabilized values obtained after repeated sample exposure to light, reveals the order Cu > Ni > Fe > platinized Pt for the relative effectiveness of these four metals as counterelectrodes in reaction 4 at current densities of ~1 $\mu A/cm^2$. Scans taken in the opposite direction, i.e., beginning at the short-wavelength end, yielded the same ordering of maximum photocurrents due to different anode materials, with the overall values in this case decreasing as the red maximum is approached.

The decay with light exposure of the photocurrent at 735 nm is examined as a function of the wavelength and intensity of laser light employed in illuminating the *n*-pentane (Chl $a \cdot 2H_2O)_n$ suspension during the plating procedure. The data, obtained under three different sets of illumination conditions at the same plating field, 1300 V/cm, are shown in Figure 8. These data correspond to the maximum value of the observed photocurrent, using a Cu counterelectrode, at the onset of repetitive 10-s exposures similar to those given in Figure 5 for a Pt/Chl *a* electrode prepared under white light illumination. The 10-s light periods were interposed by 40-s dark intervals (not shown). The time coordinate in Figure 8 measures only the additive duration of sample exposure to 735-nm light. The data obtained by using the Ar ion laser line

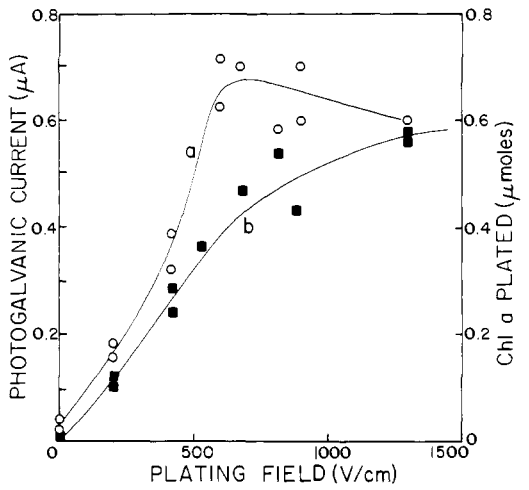

Figure 9. (a) Photogalvanic outputs of Pt/Chl a electrodes prepared under illumination by a 2-mW 632.8-nm He-Ne laser beam at various plating fields. (b) Amounts of Chl on a plated on a 1.0 × 1.0 cm^2 Pt foil at various plating fields.

at 514.5 nm are numerically fitted to general expressions of the type

$$i_p = \beta(1 + \gamma e^{-kt}) \quad (7)$$

where the photocurrent, i_p, is seen to decay from an initial value, $i_{p,0} = \beta(1 + \gamma)$, to a constant level, $i_{p,\gamma} = \beta$, at long times. The two fits a and b bracket the data obtained from a plating procedure employing 2-mW He–Ne laser illumination at 632.8 nm for which a similar fit (not shown) is also observed. From these fits we find that the decay constant k and initial photocurrents, $i_{p,0}$, are evidently functions of both the wavelength and the intensiy of illumination to which the sample plating procedure was subjected.

The dependence of the photogalvanic current on the potential field employed in the electroplating procedure is given in Figure 9a. The data were obtained by using a Cu counterelectrode. The Pt/Chl a electrode was prepared under illumination at 632.8 nm by a 2-mW He–Ne laser. The plating process was allowed to proceed for 10 min. A maximum photocurrent, 0.72 μA, was observed at 615 V/cm, corresponding to a conversion quantum efficiency of 0.88% at an incident (735 nm) flux of 1.7 × 10^{15} photons/s. At 1500 V/cm dielectric breakdown caused arcing across the plating chamber, setting an upper limit for the range of applied fields investigated. Figure 9b shows the amount of Chl a deposited on a Pt electrode as a function of the plating field. At 815 V/cm a coverage of 5.4 × 10^{-7} mol of Chl a was found, corresponding to ~10^3 Chl a monolayers.

In Figure 10 electron micrographs of typical Pt/Chl a electrode surfaces prepared under different plating fields are shown. Figure 10a demonstrates the appearance, magnified 1596×, of a (Chl a·$2H_2O$)$_n$ surface prepared at an applied field of 1300 V/cm, under illumination by a 20-mW output of the 514.5-nm Ar ion laser line. The appearance of a beehive-like substructure in the granular surface gives evidence of the fusion of (Chl a·$2H_2O$)$_n$ microcrystals as they are deposited on the Pt foil under the applied field. Figure 10b is an enlarged view of Figure 10a, shown at the same magnification (5130×) as the micrograph (Figure 10c) of another area of the same electrode surface, in which the chlorophyll microcrystals have apparently disintegrated in a reorganization of the Pt/Chl a electrode surface structure. The formation of a contiguous (Chl a·$2H_2O$)$_n$ multilayer is shown in Figure 10d for a Pt/Chl a electrode prepared at 615 V/cm corresponding to the optimum plating field at which the photogalvanic output of 4 is at a maximum (Figure 9).

The light and dark ESR spectra of 1.0 × 10^{-3} M Chl a solution in water-saturated n-pentane in the presence and absence of 1 atm of H_2 are shown in Figure 11. From optical spectrometric measurement it was observed that the sample solution consisted predominantly of (Chl a·$2H_2O$)$_n$ having a red absorption maximum at 743 nm. Less than 5% of the chlorophyll existed in the form of monomeric Chl a, which is characterized by its red absorption maximum at 662 nm.[13] The ESR peak-to-peak widths are 4.9 G for the light signal and 10.6 G for the dark signal. A corresponding width of 5.1 G was obtained for the light-minus-dark signal which decays according to the empirical expression (see dotted fit in inset of Figure 11)

$$C^+(t) = \langle C^+ \rangle (0.25e^{-t/0.2} + 0.75e^{-t/1.7}) \quad (8)$$

where $\langle C^+ \rangle$ and $C^+(t)$ are, respectively, the steady-state concentration under illumination and the concentration after illumination of (Chl a·$2H_2O$)$_n^+$· responsible for the observed ESR signal. The ratio of areas, $\alpha = \alpha_L/\alpha_D$, under the light-minus-dark and the dark spectra is 1.12. The g values for the dark and light-minus-dark signals are 2.0030 and 2.0025, respectively. The concentration, C^+, of the photooxidized Chl a, according to the intensity of the light-minus-dark ESR signal, was found to be 2.6 × 10^{-6}, M using DPPH as standard under saturating illumination conditions (104 mW/cm^2). In the presence of H_2 the narrow-width (5.1 G) signal was not observed in the light-minus-dark spectrum.

The flux dependence of the difference between the potential of Pt/Chl a vs. Pt/H_2 measured under illumination and that observed in the dark is shown in Figure 3. The EMF's in the dark and the strong light limit (104 mW/cm^2) of the cell, Pt|H_2(1 atm)–H_2O, 0.5 M KCl–(Chl a·$2H_2O$)$_n$|Pt, in which Pt|Chl a·$2H_2O$)$_n$ is the cathode, are 0.693 and 0.813 V, respectively. The corresponding EMF's in the absence of H_2 are −0.036 and 0.038 V, respectively.

Discussion

(i) Characterization of Chl *a* Multilayers on Pt. The observation of a plating current in the absence of light (Figure 4b) reflects the presence of Chl a^+· radical cations in the dark, as shown in Figure 11. The ratio of areas under the dark and the light-minus-dark plating current–time curve is ~0.8, in fair agreement with the corresponding ESR area ratio, α = 1.1, of Figure 11. The observtion of a 10.6-G line width for the dark ESR signal (Figure 11b) indicates the presence of monomeric radical cations.[22] The 0.2- and 1.7-s lifetimes in eq 8 suggest the dimeric and hexameric origins of the light-minus-dark ESR spectrum in Figure 11c, in accordance with earlier determinations.[31] From the known[31] line widths, 7.5 and 4.3 G, respectively, for (Chl a·$2H_2O$)$_2^+$· and Chl a·$2H_2O$)$_6^+$·, and the corresponding weighting factors, 0.25 and 0.75 in eq 8, we obtain an estimated width, 5.1 G, for the composite ESR signal, in agreement with the observed line width. The weighted apparent aggregate size of (Chl a·$2H_2O$)$_n^+$· is thus given by $\langle n \rangle \sim 5$. Assuming this number to be the average aggregate size, the concentration, C_0, of (Chl a·$2H_2O$)$_n$ in the sample solution is estimated to be about 1.9 × 10^{-4} M. The ratio $C^+/C^0 = 1.3 \times 10^{-2}$ is thus obtained from ESR observations for the fraction of (Chl a·$2H_2O$)$_n$ photooxidized under saturating light conditions.

The mass spectrometric observation of H_2 and O_2 supports the water photolytic origin of the photogalvanic currents shown in Figure 5–9. The kinetic effects of the photocurrent shown in Figure 6 are thus manifestations of the secondary processes of the Chl a light reaction responsible for oxygen evolution from water photolysis. The dependence of the initial photocurrent $\beta(1 + \gamma)$ on the intensity and wavelength of illumination during the photoelectrodeposition procedure (Figure 8) appears to be compatible with the greater extent of (Chl a·$2H_2O$)$_n$ photooxidation at higher light fluxes and, in view of Figure 7, of the higher extinction coefficient or photocatalytic activity of (Chl a·$2H_2O$)$_n$ at 632.8 nm than that at 514.5 nm.

The increase in the amount of Chl a electrodeposited as the plating field is increased (Figure 9b) is indicative of mass transport controlled deposition.[23] This observation is comparable to recent results reported by Miyasaka et al.[24] using Chl a multilayers on

(22) B. D. C. Borg, J. Fajer, R. H. Felton, and D. Dolphin, *Proc. Natl. Acad. Sci. U.S.A.*, **67**, 813 (1970).
(23) J. Newman, "Electrochemical Systems," Prentice-Hall, Englewood Cliffs, NJ, 1973, p 297.

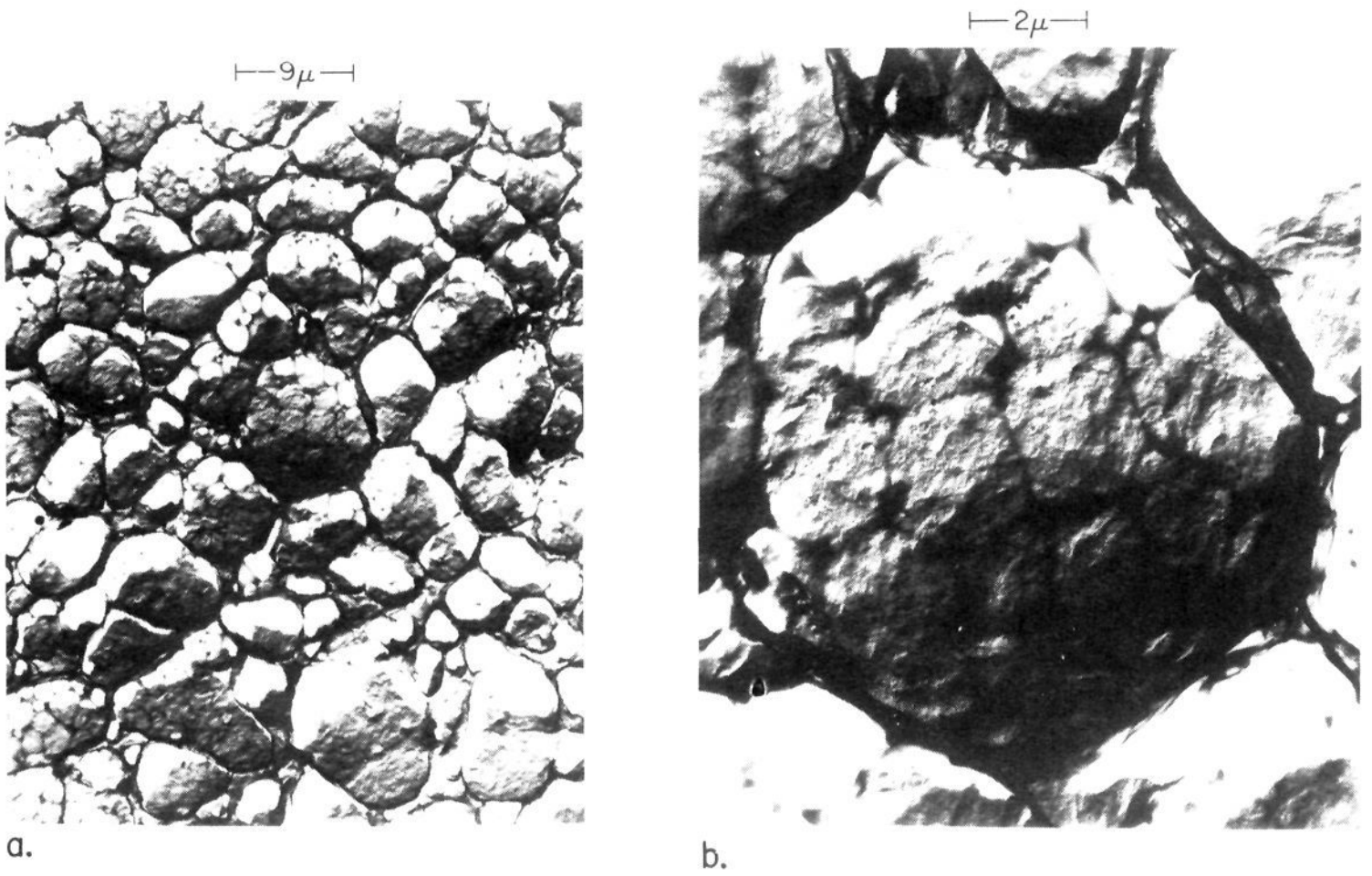

Figure 10. Electron micrographs of Pt/Chl *a* electrode surfaces prepared at two different plating fields: (a) Pt/Chl *a* electrode prepared at 1300 V/cm with a 20-mW Ar ion laser beam at 514.5 nm, magnified 1596×. The average diameter of the larger crystals is ~9.4 μm. (b) Same surface area as in a, magnified 5130×. The subunits in the beehive-like structure have an average diameter of ~2.4 μm. (c) A different location of the same Pt/Chl *a* surface as in a, magnified 5130×. (d) A second Pt/Chl *a* electrode surface prepared under the same illumination conditions as the sample in a but at a lower plating field of 680 V/cm, magnified 1596×.

SnO_2. Comparison of Figure 10a to 10d indicates a change in the morphology and characteristics of the deposit reminiscent of the experimental behavior observed in the mass transport mediated electrodeposition of metals. As the limiting current is approached in the latter case, particle size is reduced, resulting in a fine, compact, powdery deposit.[25,26] The metal deposits thus obtained consist of particles having diameters on the order of 0.1 μm and show greater reactivity in hydrogenation-type reations due to the small particle size.[27] Also, it has been established that the current distribution for vertical electrodes is uniform at $^1/_3$–$^1/_2$ of the limiting current value.[28] As the plating field is increased and the limiting current is approached, the current distribution around the Pt cathode becomes markedly nonuniform due to increased

(24) T. Miyasaki, T. Watanabe, A. Fujishima, and K. Honda, *Photochem. Photobiol.*, **32**, 217 (1980).
(25) N. Ibl, *Adv. Electrochem. Electrochem. Eng.*, 2, 49 (1962).
(26) N. Ibl, *Chem. Ind. (London)*, **8**, 326 (1975).
(27) W. Eckardt, *Inf. Circ.*, U.S., *Bur.* Mines **No. 7466** (1948); *Chem. Abstr.*, **45**, 6089 (1951).
(28) C. J. Wagner, *Electrochem Soc.*, **104**, 129 (1957).

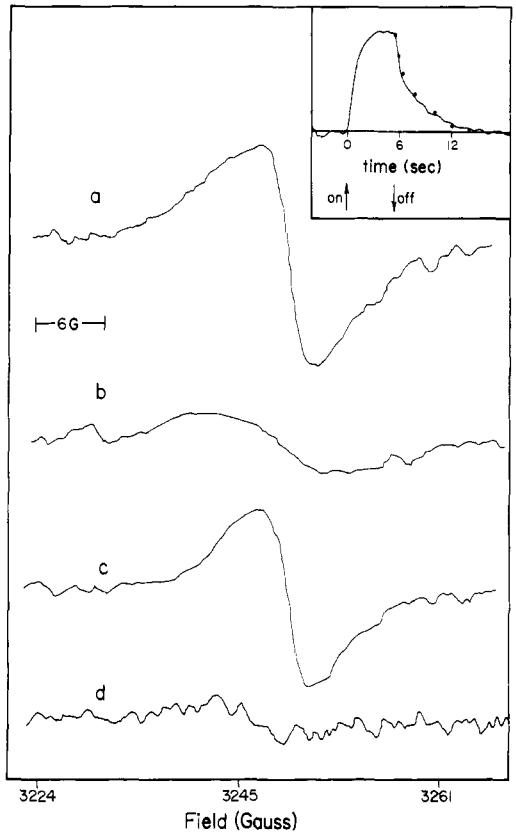

Figure 11. Electron spin resonance spectra of 1.0×10^{-3} M Chl *a* in water-saturated *n*-pentane solution: (a) light; (b) dark; (c) light-minus-dark spectra in the absence of H_2; (d) light-minus-dark spectrum under 1 atm of H_2. Modulation = 1.6 G, gain = 2.5×10^4, microwave power = 12.5 mW, frequency = 9.08 GHz, incident light flux = 104 mW/cm^2. Inset: kinetic behavior of the light-minus-dark spectrum corresponding to c.

convection in the bulk medium. A comparison of the plots in Figure 9, a and b, suggests a relationship between the photocurrent and the physical state of the chlorophyll deposited on the Pt substrate. It appears likely that at fields >700-V/cm hydrodynamic factors (i.e., increased convection) would result in a disparate structure of the electrodeposited Chl *a*. A nonuniform surface consisting of powdery Chl *a* at the top and a compact, adherent deposit toward the bottom of a vertical Pt electrode is observed (Figure 10a–c) analogous to Cu deposition under natural convection.[25] The concomitant disorder in the multilayer film as the plating field is increased possibly results in a lowering of the efficiency of quantum conversion by the chlorophyll.

In Figure 9a the maximum photocurrent, 0.72 μA, observed on 735-nm photoexcitation of samples prepared under optically controlled conditions, corresponds to a quantum efficiency of 0.88%, more than four times that, 0.21%, observed for a Pt/Chl *a* electrode prepared under white light illumination (see, Pt/Chl *a* vs. Cu, Figure 7). In earlier work using shiny Pt as counterelectrode and uncontrolled plating procedures, quantum efficiencies at 735 nm in the 0.02[29] –0.06%[14] range were reported.

The rise and subsequent decay to a steady-state value in the photocurrent, shown in Figure 6, offers a kinetic view of reaction 6 which supplies the electrons for reducing the photooxidized Chl *a* at the photocathode. The ~1-ms rise time is several orders of magnitude longer than the ~1-ns current component observed when condensed (Chl *a*·$2H_2O$)$_n$ is excited by a pulsed source.[30] Significantly, the fast component, attributed to a charge separation mechanism of the Chl *a* film, also displays a saturation phenomenon similar to that shown in Figure 5 on repetitive excitation.

(ii) Kinetic Model for Oxygen and Hydrogen Evolution. The presence of oxygen at the counterelectrode quenches[14] the photogalvanic output of 4. It has been established that the addition of an O_2 scavenger to the anode compartment significantly enhances the observed photocurrents.[31] The results shown in Figure 5 for the decay of the photogalvanic activity with light exposure and subsequent restoration of this activity on purging with Ar gas suggests a possible interpretation for the exponential decay, according to eq 7, of the photocurrent to a constant steady-state value at long exposure times. Assuming that reaction 6 is the primary source of electrons on photoactivation of the half-cell reaction 5 at the Pt/Chl *a* electrode, we write for the rate of oxygen accumulation at the counterelectrode

$$\frac{d\eta_{ox}}{dt} = \alpha I_0 C_0(1 - \eta_{ox}) - D\eta_{ox} \tag{9}$$

where α is a proportionality constant, I_0 and C_0 are, respectively, the incident flux and the number of Chl *a* molecules engaged in photogalvanic conversion, η_{ox} is the fraction of the catalytically active sites at the counterelectrode incapacitated by oxygen coverage, and D is a rate parameter related to the process of oxygen liberation through diffusion and/or convection from the counterelectrode. On solving eq 8 we obtain

$$\eta_{ox}(t) = \alpha I_0 C_0(1 - e^{-k't})/k' \tag{10}$$

where

$$k' = \alpha I_0 C_0 + D \tag{11}$$

This equation is valid only for constant light on–off cycles with total exposure times $\lesssim$10 min. The decay of the photocurrent from its initial value, $i_{p,0}$, as a result of oxygen accumulation at the counterelectrode is thus given by

$$i_p(t) = i_{p,0} - f\eta_{ox} = \beta'(1 + \gamma' e^{-k't}) \tag{12}$$

where f is a proportionality constant and β' is the stabilized photocurrent obtained at long times:

$$i_{p,\infty} = \beta' = i_{p,0} - \alpha f I_0 C_0/(\alpha I_0 C_0 + D) \tag{13}$$

In eq 12 the coefficient γ' is written as

$$\gamma' = \alpha f T_0 C_0/k'(i_{p,0} - \alpha f I_0 C_0/k') \tag{14}$$

It is evident that eq 12 is compatible with the numerical fit in eq 7 for the experimental data shown in Figure 7.

In addition to the effects attributed to O_2, H_2 inhibition of the photogalvanic action must also be considered (see iv). A kinetic model along the lines developed above is thus expected to be applicable to H_2 evolution off the Pt/Chl *a* electrode.

(iii) Oxygen Overvoltages of Different Anode Metals. According to eq 13 the stabilized photocurrent, $i_{p,\infty}$, increases with increasing values of the oxygen liberation rate parameter D. On the other hand, the overvoltage for oxygen evolution varies inversely as the oxygen liberation rate. The order Cu > Ni > Fe > plainized Pt > Pt for the relative effectiveness of these metals as counterelectrodes in (4), derived from the observed stabilized photocurrents in Figure 7 and data obtained by using shiny Pt as counterelectrode,[14] thus suggests a corresponding order Pt > platinized Pt > Fe > Ni > Cu for the overvoltages of oxygen-depleted environment, consistent with previous observations. This ordering provides a comparison and extrapolation for the overvoltages of oxygen evolution reported[32] for current densities in excess of 10 μA/cm^2 in oxygen-saturated aqueous solutions and is consistent with proposed models of oxygen evolution from metal bonds.[33] From considering the standard oxidation potentials one would expect that, for Fe, Ni, or Cu, anodic dissolution is favored over water oxidation. However, appreciable dissolution was not observed for any of the metals employed as anodes in the pho-

(29) L. M. Fetterman, L. Galloway, N. Winograd, and F. K. Fong, *J. Am. Chem. Soc.*, **99**, 653 (1977).
(30) A. Bromberg, C. W. Tang, and A. C. Albert, *J. Chem. Phys.*, **60**, 4058 (1974).
(31) P. Delahay "Double Layer and Electrode Kinetics", Interscience, New York, 1965, p 260.
(32) A. Hickling and S. Hill, *Faraday Soc. Discuss.* 1 (1947).
(33) S. Glasstone "An Introduction to Electrochemistry", Van Nostrand, New York, 1942, p 447.

togalvanic experiment. While anodic dissolution undoubtedly occurs when the cell using a Fe, Ni, or Cu anode is first assembled and connected to the external circuit, the increase in current density upon illumination of the Pt/Chl *a* electrode renders the anode passive. This is attributed to the production of an "adherent and invisible" oxide coat which inhibits dissolution of the metal and promotes oxygen evolution.[33] Platinum is generally regarded as unattackable and is nearly always in the passive state.

(iv) Cathodic Photopotential of the Pt\|(Chl *a*·2H$_2$O)$_n$ Electrode. Using the H_2 electrode as reference half-cell the EMF's of the Pt/Chl *a* cell in the dark and in the strong light limit are respectively 0.69 and 0.81 V at pH 6.2 (Figure 3). In the absence of H_2 the measured EMF's of the cell in Figure 3 differ significantly from these values, as is to be expected on account of the fact that they are attributable to redox reactions between, instead of H_2, the aqueous solution and the chlorophyll. The observed change in sign of the EMF, from anodic (−0.036 V) to cathodic (0.038 V) behavior of Pt/Chl *a* in transition from darkness to conditions of light, underscores the ESR observation of monomeric Chl $a^{+}\cdot$ in the dark and that of (Chl *a*·2H$_2$O)$_n^{+}\cdot$ only in the light (Figure 11). The observation of the anodic photopotential in the dark may be rationalized in terms of the oxidation of Chl *a* by water and/or oxygen on establishment of an equilibrium concentration of Chl $a^{+}\cdot$ in the unpoised Pt/Chl *a* electrode. The generation of a cathodic photopotential at an illuminated Pt/Chl *a* electrode can be specially accounted for by the oxidation of H_2O by (Chl *a*·2H$_2$O)$_n^{+}\cdot$ radical cations produced on photooxidation of the chlorophyll dihydrate aggregates:

$$(\text{Chl } a\cdot 2H_2O)_n^{+}\cdot + {}^1/_2H_2O \rightarrow (\text{Chl } a\cdot 2H_2O)_n + {}^1/_4O_2 + H^+ \quad (15)$$

The occurrence of reaction 15 is supported by (i) the observed decay of only the (Chl *a*·2H$_2$O)$_n^{+}\cdot$ ESR signal (light-minus-dark) when the light is turned off (inset, Figure 11), (ii) the mass spectrometric observation of oxygen evolution from deoxygenated Pt\|(Chl *a*·2H$_2$O)$_n$ sample cells,[16,17] and (iii) the 740-nm maximum in the photocathodic current action spectrum.[14] The light-minus-dark EMF, 0.038 V − (−0.036 V) may accordingly be taken to be the photo-EMF, E_L, for reaction 15

$$E_L = 0.074 = E^0 + E'_{H_2O/O_2} - (RT/F)\ln (C^0/C^+)[H^+]P_{O_2}{}^{1/4} \quad (16)$$

where E^0 is the standard reduction potential of (Chl *a*·2H$_2$O)$_n^{+}\cdot$, $E'_{H_2O/O_2} = -1.23$ V is the oxidation potential of H_2O at $P_{O_2} = 1$ atm of O_2 and pH 0, and $C^+/C^0 \sim 10^{-2}$ is the ratio observed from Figure 11 for the faction of (Chl *a*·2H$_2$O)$_n$ photooxidized under saturating light conditions [see (i)]. From eq 16 we obtain $E^0 \simeq 1.05$ V, which is to be compared to the value, 0.92 V, reported earlier for the reduction potential of (Chl *a*·2H$_2$O)$_n^{+}\cdot$ in 1:1 acetone–water.[34] The photo-EMF measured in the presence of 1 atm of H_2 arises from redox reactions different from reaction 15. The absence of the 5.1-G signal in the light-minus-dark ESR spectrum measured in the presence of H_2 (Figure 11) indicates that (Chl *a*·2H$_2$O)$_n^{+}\cdot$ radical cations are not obtainable under the reducing atmosphere of H_2. On the basis of published Chl *a* potentials[35] the cathodic potential, 0.69 V, measured in the dark may be ascribed to the reduction of monomeric Chl $a^{+}\cdot$ by H_2. Likewise, the photocathodic potential, 0.12 V, obtained from the light-minus-dark difference EMF could possibly be due to excited Chl *a* reduction by H_2 to yield the radical anion, Chl $a^{-}\cdot$.[35] In a related study the EMF's of Chl *a* multilayers on SnO_2 were measured against a standard calomel cell.[24] The present considerations emphasize the choice of reference half-cells in determining Chl *a* redox properties on account of the variety of Chl *a* redox couples and the Chl *a* reaction-pathway dependence on the chlorophyll's aggregation state.

The photogalvanic current decay (Figure 6) is about three orders of magnitude faster than the corresponding decay of the ESR signal shown in Figure 11. This difference is attributable to the presence of the metal counterelectrode acting as catalyst for the oxygen evolution from water splitting in the photogalvanic experiment. The P680 photoreaction cycle occurs on a μs time scale,[36] three orders of magnitude yet faster than the Chl *a* cycle given in Figure 6. The narrowing of the gap in Chl *a* reaction cycle times in vivo and in vitro appears to be an important goal for future work in this research field.

Acknowledgment. The work reported in this paper was supported by the Basic Research Division of the Gas Research Institute. The work in the "Discussion" section on the reduction potential of (Chl *a*·2H$_2$O)$_n$ was conceived as a result of discussions that took place during the GRI sponsored photochemistry meeting in Albuquerque, NM, April 21–22, 1981.

(34) L. Galloway, J. Roettger, D. R. Fruge, and F. K. Fong, *J. Am. Chem. Soc.*, **100**, 4635 (1978).
(35) G. R. Seely, *Photochem. Photobiol.*, **27**, 639 (1978).
(36) M. Glaser, Ch. Wolf, and G. Renger, *Z. Naturforsch, C*, **31**, 712 (1976); J. A. Van Best, P. Mathis, *Biochim. Biophys. Acta*, **503**, 178 (1978); A. Sonneveld, H. Rademaker, and L. N. M. Duysens, *Biochim. Biophys. Acta*, **548**, 536 (1979).